13. Penrose, O. & Onsager, L. Bose Einstein condensation and liquid helium. *Phys. Rev.* **104,** 576–584 (1956).
14. Wyatt, A. F. G. Liquid ^{4}He: An ordinary and exotic liquid. *J. Phys.: Condens. Matter* **8,** 9249–9262 (1996).
15. Krotscheck, E. Liquid helium on a surface: ground state, excitations, condensate fraction and impurity potential. *Phys. Rev. B* **32,** 5713–5730 (1985).
16. Campbell, C. E. Remnants of Bose condensation and off-diagonal long range order in finite systems. *J. Low Temp. Phys.* **93,** 907–919 (1993).
17. Griffin, A. & Stringari, S. Surface region of superfluid helium as an inhomogeneous Bose-condensed gas. *Phys. Rev. Lett.* **76,** 259–263 (1996).
18. Sears, V. F., Svensson, E. C., Martel, P. & Woods, A. D. B. Neutron-scattering determination of the momentrum distribution and condensate fraction in liquid ^{4}He. *Phys. Rev. Lett.* **49,** 279–282 (1982).
19. Sears, V. F. Kinetic energy and condensate fraction of superfluid ^{4}He. *Phys. Rev. B* **28,** 5109–5121 (1983).
20. Ceperley, D. M. & Pollock, E. L. Path integral computation of the low-temperature properties of liquid ^{4}He. *Phys. Rev. Lett.* **56,** 351–354 (1986).
21. Manousakis, E. Pandharipande, V. R. & Usmani, Q. N. Condensate fraction and momentum distribution of the ground state of liquid ^{4}He. *Phys. Rev. B* **31,** 7022–7028 (1985).
22. Whitlock, P. A. & Panoff, R. M. Accurate momentum distributions from computations on ^{3}He and ^{4}He. *Can. J. Phys.* **65,** 1409–1415 (1987).
23. Tucker, M. A. H. & Wyatt, A. F. G. Phonons in liquid ^{4}He from a heated metal film: I. The creation of high-frequency phonons. *J. Phys.: Condens. Matter* **6,** 2813–2824 (1994).
24. Tucker, M. A. H. & Wyatt, A. F. G. Phonons in liquid ^{4}He from a heated metal film: II The angular distribution. *J. Phys.: Condens. Matter* **6,** 2825–2834 (1994).
25. Edwards, D. O. & Saam, W. F. The free surface of liquid helium. *Prog. Low Temp. Phys.* **7,** 283–369 (1978).

Acknowledgements. I thank A. Griffin for encouragement and for comments on the draft manuscript; C. Williams and J. Warren for discussions on their results for ^{3}He and allowing me to quote them; C. Williams and M. Brown for the simulation of the peak in Fig. 1; and M. Gibbs for discussions on neutron scattering. This work was supported by the EPSRC.

Correspondence should be addressed to the author (e-mail: A.F.G.Wyatt@exeter.ac.uk).

Electronic structure of atomically resolved carbon nanotubes

Jeroen W. G. Wildöer*, Liesbeth C. Venema*, Andrew G. Rinzler†, Richard E. Smalley† & Cees Dekker*

** Department of Applied Physics and DIMES, Delft University of Technology, Lorentzweg 1, 2628 CJ Delft, The Netherlands*
† Center for Nanoscale Science and Technology, Rice Quantum Institute, Departments of Chemistry and Physics, MS-100, Rice University, PO Box 1892, Houston, Texas 77251, USA

Carbon nanotubes can be thought of as graphitic sheets with a hexagonal lattice that have been wrapped up into a seamless cylinder. Since their discovery in 1991[1], the peculiar electronic properties of these structures have attracted much attention. Their electronic conductivity, for example, has been predicted[2–4] to depend sensitively on tube diameter and wrapping angle (a measure of the helicity of the tube lattice), with only slight differences in these parameters causing a shift from a metallic to a semiconducting state. In other words, similarly shaped molecules consisting of only one element (carbon) may have very different electronic behaviour. Although the electronic properties of multi-walled and single-walled nanotubes[5–12] have been probed experimentally, it has not yet been possible to relate these observations to the corresponding structure. Here we present the results of scanning tunnelling microscopy and spectroscopy on individual single-walled nanotubes from which atomically resolved images allow us to examine electronic properties as a function of tube diameter and wrapping angle. We observe both metallic and semiconducting carbon nanotubes and find that the electronic properties indeed depend sensitively on the wrapping angle. The bandgaps of both tube types are consistent with theoretical predictions. We also observe van Hove singularities at the onset of one-dimensional energy bands, confirming the strongly one-dimensional nature of conduction within nanotubes.

As shown in Fig. 1A, a carbon nanotube can be constructed by wrapping up a single sheet of graphite such that two equivalent sites of the hexagonal lattice coincide. The wrapping vector **C**, which defines the relative location of the two sites, is specified by a pair of integers (n,m) that relate **C** to the two unit vectors $\mathbf{a}_1$ and $\mathbf{a}_2$ ($\mathbf{C} = n\mathbf{a}_1 + m\mathbf{a}_2$). A tube is called 'armchair' if n equals m, and 'zigzag' in the case $m = 0$. All other tubes are of the 'chiral' type and have a finite wrapping angle ϕ with $0° < \phi < 30°$ (ref. 13). To be

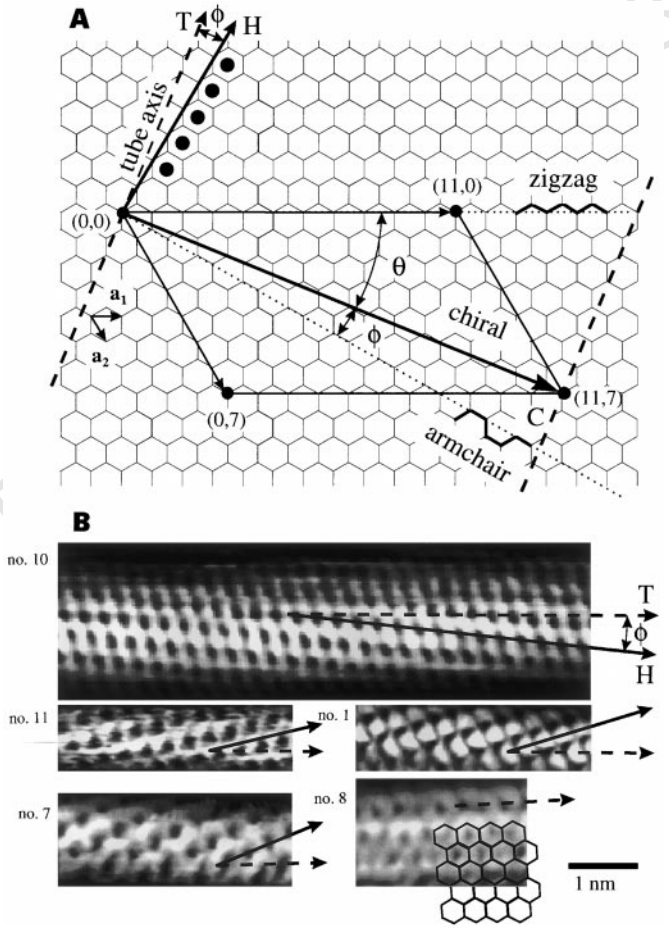

Figure 1 Relation between the hexagonal carbon lattice and the chirality of carbon nanotubes. **A**, the construction of a carbon nanotube from a single graphene sheet. By rolling up the sheet along the wrapping vector **C**, that is, such that the origin (0,0) coincides with point C, a nanotube indicated by indices (11,7) is formed. Wrapping vectors along the dotted lines lead to tubes that are zigzag or armchair. All other wrapping angles lead to chiral tubes whose wrapping angle is specified relative to either the zigzag direction (θ) or to the armchair direction ($\phi = 30° - \theta$). Dashed lines are perpendicular to **C** and run in the direction of the tube axis indicated by vector **T**. The solid vector **H** is perpendicular to the armchair direction and specifies the direction of nearest-neighbour hexagon rows indicated by the black dots. The angle between **T** and **H** is the chiral angle ϕ. **B**, Atomically resolved STM images of individual single-walled carbon nanotubes. The lattice on the surface of the cylinders allows a clear identification of the tube chirality. Dashed arrows represent the tube axis **T** and the solid arrows indicate the direction of nearest-neighbour hexagon rows **H**. Tubes no. 10, 11 and 1 are chiral, whereas tubes no. 7 and 8 have a zigzag and armchair structure, respectively. Tube no. 10 has a chiral angle $\phi = 7°$ and a diameter $d = 1.3$ nm, which corresponds to the (11,7) type of panel **A**. A hexagonal lattice is plotted on top of image no. 8 to clarify the non-chiral armchair structure. Carbon nanotubes were synthesized as described in ref. 14. TEM studies[14] have shown that the material consists mainly of ~1.4-nm-thick single-walled nanotubes. These were deposited from a dispersion in 1,2 dichloroethane on single-crystalline Au(111) facets. Topographic images were obtained by recording the tip height at constant tunnel current in a home-built STM[25] operated at 4 K. The Pt/Ir tips were cut in ambient air by scissors. Typical bias parameters are those of image no. 10, that is, a tunnel current $I = 60$ pA, and a bias voltage $V_{bias} = 500$ mV.

able to correlate the electronic properties of a tube with its atomic structure, atomically resolved images are required. In Fig. 1B we show examples of such scanning tunnelling microscopy (STM) images of single-wall carbon nanotubes. (The chiral angle $\phi = 7°$, and diameter $d = 1.3$ nm of tube no. 10 correspond to vector $C = (11, 7)$ in the top panel of Fig. 1.)

The critical dependence of the electronic spectra of nanotubes on the tube indices (n, m) can be understood by again taking the two-dimensional graphene sheet as a starting point. In the circumferential direction (along **C**), periodic boundary conditions apply, that is, $\mathbf{C}\cdot\mathbf{k} = 2\pi q$ (ref. 13), where **k** is the wavevector and q is an integer. This leads to a set of allowed values for **k** which can be substituted into the energy dispersion relation for a graphene sheet to yield the dispersion relations for the tube, with q labelling the various one-dimensional modes. Calculations[13] predict that armchair $(n = m)$ tubes have bands crossing the Fermi level and are therefore metallic. For all other tubes (chiral and zigzag) there exist two possibilities. When $n - m = 3l$ (where l is an integer), tubes are also expected to be metallic. In the case $n - m \neq 3l$, tubes are predicted to be semiconducting with an energy gap of the order of ~0.5 eV. This gap should only depend on the diameter, that is, $E_{gap} = 2\gamma_0 a_{C-C}/d$, where γ_0 is the C–C tight-binding overlap energy, a_{C-C} the nearest-neighbour C–C distance (0.142 nm) and d the diameter.

Atomic resolution was achieved on more than 20 tubes, corresponding to ~80% of the tubes investigated. In most cases only a few rows of atoms on top of the tube could be imaged. Very few armchair tubes were observed, which is in apparent contrast with earlier investigations on the same type of material[14,15]. However, unlike these earlier experiments we have concentrated on individual tubes, and have neglected the ropes of tubes.

Figure 1B shows atomically resolved STM images on five different tubes. The most prominent feature is the triangular lattice of dark dots with a lattice spacing of ~0.25 nm, as expected for a graphene lattice. We attribute the dark dots to the centres of the hexagons[16]. The atomic resolution images allow us unambiguously to determine the chiral angle, that is, the angle between the hexagon rows and the

Table 1 Overview of the experimental STM and STS results on individual single-walled carbon nanotubes

Tube number	1	2	3	4	5	6	7	8	9	10	11	12	13	14	15	16	17	18	19	20	21	22	23	24	25	26	27
Chiral angle ϕ (deg)	25	4	7	24	9	14	30	0		7	14		7	16		4	9	16	6	29	16	18	9	7	28	27	6
Diameter d (nm)	1.4	1.4	2.0	1.2	1.7	1.3	1.1	1.3	1.3	1.3	1.3	1.5	1.5	1.4	1.4	1.4	1.4	1.2	1.3	1.3	1.9	1.0	1.4	1.5	1.7	1.4	1.4
E_{gap} (eV)	0.55	0.60	0.50	0.65	1.7	1.8	1.9		0.65			1.8	2.0	1.9	0.60	0.5	0.55	0.60	0.60	0.5	0.4						
δE (eV)	0.25	0.3	0.25	0.3	0.3	0.2	0.2		0.30			0.3	0.4	0.3	0.30	0.2	0.30	0.30	0.30	0.2	–0.2*						

Here d is the nanotube diameter; ϕ is the chiral angle; E_{gap} is the apparent bandgap in the STS I–V spectra and δE is the shift of the Fermi energy due to doping of the tube by the substrate. Note that a chiral angle of 0° denotes an armchair nanotube, and an angle of 30° a zigzag tube. The flat Au surface allowed the diameter d of the nanotubes to be determined with an accuracy of 0.1 nm by measuring the tube heights relative to the surface. A possible systematic uncertainty in determining the diameter is due to a difference in barrier heights for the gold substrate and the tubes. The wrapping angle ϕ can be determined with an accuracy of ~1°. Accuracy in ϕ is limited by the curvature of the tubes. A combination of high accuracy in both ϕ (~1°) and d (~0.05 nm) is required for an unambiguous identification of the n, m indices. Accuracy in E_{gap} and δE is 0.05–0.1 eV.
* For this sample we observed a shift in the Fermi energy towards the conduction band, instead of a shift towards the valence band as observed in the other samples. We speculate that the gold substrate for this sample may have had an anomalously low work function.

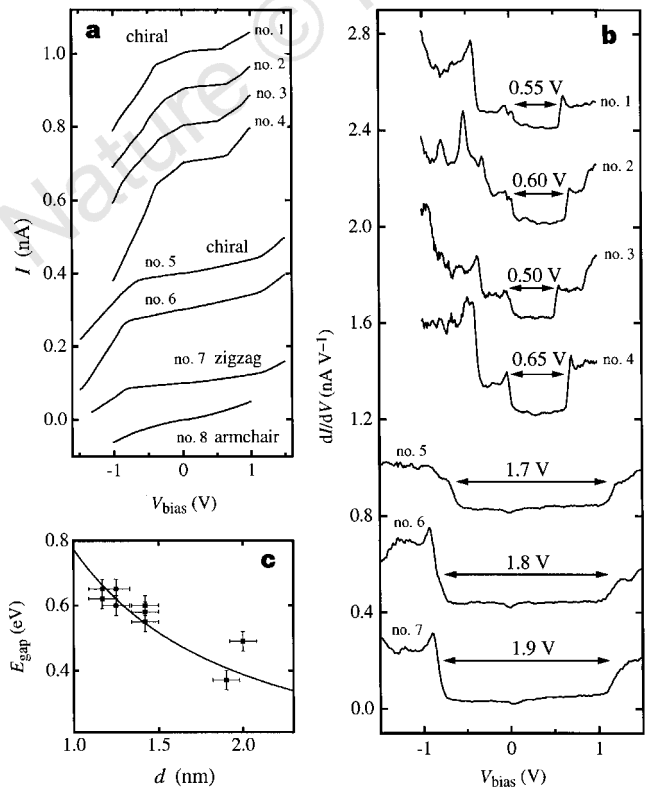

Figure 2 Electronic properties of single-walled carbon nanotubes. **a**, Current–voltage curves obtained by tunnelling spectroscopy on various individual nanotubes. Tubes nos 1–6 are chiral, no. 7 is zigzag and no. 8 is armchair. The bias voltage is applied to the sample, which means that the sign of V_{bias} corresponds to that of the energy relative to the tube Fermi level. Curves nos 1–7 show a low conductance at low bias, followed by several kinks at larger bias voltages. The armchair tube does not show clear kinks in the range –1 to +1 V. **b**, The derivatives dI/dV. For clarity, curves are offset vertically by multiples of 0.4 nA V^{-1}. Gaps are indicated by the arrows. Two categories can be distinguished: one with gap values around 0.5–0.6 eV, the other with significantly larger gap values. The first category of tubes is identified as the semiconducting type, the second as metallic tubes. About 12 out of 18 tubes were semiconducting, in accordance with the expected ratio of 2 out of 3. We note that these tubes, besides the primary gaps, also show peaks associated with secondary and higher-order gaps. For the secondary gaps we find: 1.4 eV (no. 1), 1.1 eV (no. 2), 1.2 eV (no. 3), 1.4 eV (no. 4). All gaps seem to have shifted to the right, which indicates doping of the tubes by the substrate. We refrain from concluding a zero or finite DOS from the value of dI/dV in the gap. Possible mechanisms for a small finite dI/dV within the semiconducting gap are, for example, tip-induced band bending or residual tunnelling through the tube to the gold substrate. The doping behaviour, however, indicates a finite DOS for metallic tubes, and a zero DOS for semiconducting tubes. The small dips in dI/dV at zero bias present in some of the curves are not yet understood. The displayed dI/dV data are the result of averaging over ~50 individual I–V curves for improved signal-to-noise ratio. The individual curves all contain the same essential features. **c**, Energy gap E_{gap} versus diameter d for semiconducting chiral tubes. The data points correspond quite well to the theoretical predicted values. The solid line denotes a fit of $E_{gap} = 2\gamma_0 a_{C\text{-}C}/d$ with $\gamma_0 = 2.7$ eV. Tunnel currents I as a function of the bias voltage V applied to the sample were recorded with a home-built STM (ref. 25) while scanning and feedback were switched off. The Pt/Ir tips were cut in ambient air by scissors.

tube axis. This enables us to distinguish chiral tubes (such as shown in images nos 1, 10 and 11 in Fig. 1B) from zigzag (no. 7) and armchair (no. 8) tubes. A wide variety of chiral angles is observed (see Table 1), in contrast to earlier electron-diffraction studies on ropes of single-walled nanotubes[15].

The vacuum barrier between the STM tip and the sample forms a convenient junction for scanning tunnelling spectroscopy (STS) as it allows tunnel currents at large bias voltages. In STS, scanning and feedback are switched off, and current I is recorded as a function of the bias voltage V applied to the sample. The differential conductance (dI/dV) can then be considered to be proportional to the density of states (DOS) of the tube examined. Before and after taking STS measurements on a tube, reference measurements were performed on the gold substrate. Only when the curves on gold were approximately linear, and did not show kinks or steps, were data on a tube recorded. I–V traces were only taken far from the ends of the tube and when tubes were isolated from each other. On all the tubes reported here, STS curves taken at different positions (typically over ~40 nm) showed consistent features.

Figure 2a shows a selection of I–V curves obtained by STS on different tubes. Most curves show a low conductance at low bias, followed by several kinks at larger bias voltages. From all the chiral tubes that we have investigated, we can clearly distinguish two categories: the one has a well defined gap value around 0.5–0.6 eV, the other has significantly larger gap values of ~1.7–2.0 eV (see Table 1 and Fig. 2b). The gap values of the first category coincide very well with the expected gap values for semiconducting tubes. As illustrated in Fig. 2c, which displays gap versus tube diameter, the measurement agrees well with theoretical gap values obtained for an overlap energy $\gamma_0 = 2.7 \pm 0.1$ eV, which is close to the value $\gamma_0 = 2.5$ eV suggested for a single graphene sheet[13,17,18]. The very large gaps that we observe for the second category of tubes, 1.7–2.0 eV, are in good agreement with the values 1.6–1.9 eV that we obtain from one-dimensional dispersion relations[13] for a number of metallic tubes ($n - m = 3l$) of ~1.4 nm diameter. Metallic nanotubes are expected to have a small but finite DOS near the Fermi energy (E_F) and the apparent 'gap' is associated with DOS peaks at the band edges of the next one-dimensional modes.

The gaps seen in Fig. 2 are not symmetrically positioned around zero bias voltage. This shows that the tubes are doped by charge transfer from the Au(111) substrate. The latter has a work function of ~5.3 eV which is much higher than that of the nanotubes (which presumably is similar to the 4.5-eV work function of graphite). This shifts the Fermi energy towards the valence band of the tube. In the semiconducting tubes, the Fermi energy seems to have shifted from the centre of the gap to the valence band edge. In the metallic tubes it is shifted by ~0.3 eV, which is much lower than half of the 'gap'. This provides experimental evidence that these tubes indeed have a finite DOS within the 'gap', in contrast to the zero DOS for semiconducting tubes.

The chiral tubes thus seem to be either semiconducting or metallic, with gap values as predicted. The data provide a striking verification of the band-structure calculations of nanotube electronic properties. Our electronic spectra for armchair and zigzag tubes are also consistent with the calculations, but the small number of such tubes in our experiments prevent a more general statement. For chiral metallic tubes, it has been suggested[19] that a small (~0.01 eV) gap will open up owing to the tube curvature. We did not observe such a small gap at the centre of the large 'gap' of chiral metallic tubes. This may be attributed to hybridization between wavefunctions of the tube and the gold substrate[20] which causes smoothening of small-energy features.

Sharp Van Hove singularities in the DOS are predicted at the onsets of the subsequent energy bands, reflecting the one-dimensional character of carbon nanotubes. The derivative spectra indeed show a number of peak structures (Fig. 2b). The peaks we observe differ in height depending on the configuration of the STM tip. On semiconductors, $(dI/dV)/(I/V)$ has been argued to give a better representation of the DOS than the direct derivative dI/dV, partly because the normalization accounts for the voltage dependence of the tunnel barrier at high bias[21–24]. In Fig. 3 we show $(dI/dV)/(I/V)$ on the ordinate. Sharp peaks are observed with a shape that resembles that predicted for Van Hove singularities (see right inset of Fig. 3): with increasing $|V|$, $(dI/dV)/(I/V)$ rises steeply, followed by a slow decrease. The latter should be $\propto 1/\sqrt{|V|}$ according to the theory for the DOS near a one-dimensional band edge. The experimental peaks have a finite height and are broadened, which again can be attributed to hybridization of wave functions.

Our results constitute, to the best of our knowledge, the first experimental test of the vast amount of band-structure calculations that have appeared in recent years. The central theoretical prediction, that chiral tubes are either semiconducting or metallic depending on minor variations of wrapping angle or diameter, has been verified. □

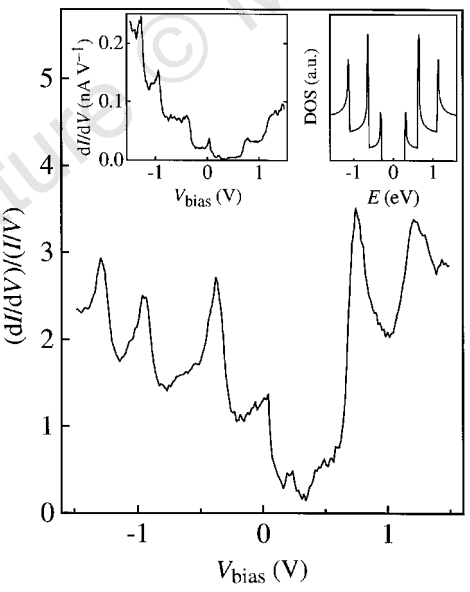

Figure 3 $(dI/dV)/(I/V)$ which is a measure of the density of states versus V for nanotube no. 9. The asymmetric peaks correspond to Van Hove singularities at the onsets of one-dimensional energy bands of the carbon nanotube. The left inset displays the raw dI/dV data. The right inset is the calculated density of states (DOS) for a (16,0) tube, which displays a typical example of the peak-like DOS for a semiconducting tube (a.u., arbitrary units). The experimental peaks have a finite height and are broadened, which we attribute to hybridization between the wavefunctions of the tube and the gold substrate. The overall shape of the experimental peaks however still resembles that predicted by theory.

Received 3 September; accepted 29 October 1997.

1. Iijima, S. Helical microtubules of graphitic carbon. *Nature* **354,** 56–58 (1991).
2. Hamada, N., Sawada, S.-I. & Oshiyama, A. New one-dimensional conductors: graphite microtubules. *Phys. Rev. Lett.* **68,** 1579–1581 (1992).
3. Saito, R., Fujita, M., Dresselhaus, G. & Dresselhaus, M. S. Electronic structure of chiral graphene tubules. *Appl. Phys. Lett.* **60,** 2204–2206 (1992).
4. Mintmire, J. W., Dunlap, B. I. & White, C. T. Are fullerene tubules metallic? *Phys. Rev. Lett.* **68,** 631–634 (1992).
5. Tans, S. J. *et al.* Individual single-wall carbon nanotubes as quantum wires. *Nature* **386,** 474–477 (1997).
6. Bockrath, *et al.* Single-electron transport in ropes of carbon nanotubes. *Science* **275,** 1922–1925 (1997).
7. Ebbesen, T. W. *et al.* Electrical conductivity of individual carbon nanotubes. *Nature* **382,** 54–56 (1996).
8. Ge, M. & Sattler, K. Vapor-condensation generation of and STM analysis of fullerene tubes. *Science* **260,** 515–518 (1993).
9. Zhang, Z. & Lieber, C. M. Nanotube structure and electronic properties probed by scanning tunneling microscopy. *Appl. Phys. Lett.* **62,** 2792–2794 (1993).
10. Ge, M. & Sattler, K. STM of single-shell nanotubes of carbon. *Appl. Phys. Lett.* **65,** 2284–2286 (1994).
11. Olk, C. H. & Heremans, J. P. Scanning tunneling spectroscopy of carbon nanotubes. *J. Mater. Res.* **9,** 259–262 (1994).

12. Carroll, D. L. *et al.* Electronic structure and localized states at carbon nanotube tips. *Phys. Rev. Lett.* **78,** 2811–2814 (1997).
13. Dresselhaus, M. S. Dresselhaus, G. & Eklund, P. C. *Science of Fullerenes and Carbon Nanotubes* (Academic, San Diego, 1996).
14. Thess, A. *et al.* Crystalline ropes of metallic carbon nanotubes. *Science* **273,** 483–487 (1996).
15. Cowley, J. M., Nikolaev, P., Thess, A. & Smalley, R. E. Electron nano-diffraction study of carbon single-walled nanotube ropes. *Chem. Phys. Lett.* **265,** 379–384 (1997).
16. Venema, L. C. *et al.* STM atomic resolution images of single-wall carbon nanotubes. *Appl. Phys. A* (in the press).
17. Mintmire, J. W., Robertson, D. H. & White, C. T. Properties of fullerene nanotubules. *J. Phys. Chem. Solids* **54,** 1835–1840 (1993).
18. White, C. T. *et al.* in *Buckminsterfullerenes* (eds Billups, W. E. & Ciufolini, M. A.) 125–184 (VCH, Weinheim, 1993).
19. Kane, C. L. & Mele, E. J. Size, shape, and low energy electronic structure of carbon nanotubes. *Phys. Rev. Lett.* **78,** 1932–1936 (1997).
20. Gadzuk, J. W. Resonance-tunneling spectroscopy of atoms adsorbed on metal surfaces: theory. *Phys. Rev. B* **1,** 2110–2129 (1970).
21. Stroscio, J. A., Feenstra, R. M. & Fein, A. P. Electronic structure of the Si(111)2 × 1 surface by scanning tunneling spectroscopy. *Phys. Rev. Lett.* **57,** 2579–2582 (1986).
22. Feenstra, R. M., Stroscio, J. A. & Fein, A. P. Tunneling spectroscopy of the Si(111)2 × 1 surface. *Surf. Sci.* **181,** 295–306 (1987).
23. Lang, N. D. Spectroscopy of single atoms in the scanning tunneling microscope. *Phys. Rev. B* **34,** R5947–R5950 (1986).
24. Hamers, R. J. in *Scanning Tunneling Microscopy and Spectroscopy* (ed. Bonnell, D. A.) 51–103 (VCH, New York, 1993).
25. Wildöer, J. W. G., van Roij, A. J. A., van Kempen, H. & Harmans, C. J. P. M. Low-temperature scanning tunneling microscope for use on artificially fabricated nanostructures. *Rev. Sci. Instrum.* **65,** 2849–2852 (1994).

Acknowledgements. The first two authors contributed equally to the present work. We thank S. J. Tans and J. C. Charlier for discussions, and L. P. Kouwenhoven, J. E. Mooij and P. M. Dewilde for support. The work at Delft was supported by the Dutch Foundation for Fundamental Research of Matter (FOM). The nanotube research at Rice was funded in part by the US NSF, the Texas Advanced Technology Program and the Robert A. Welch Foundation.

Correspondence and requests for materials should be addressed to C.D. (e-mail: dekker@qt.tn.tudelft.nl).

Atomic structure and electronic properties of single-walled carbon nanotubes

Teri Wang Odom*, Jin-Lin Huang*, Philip Kim† & Charles M. Lieber*†

** Department of Chemistry and Chemical Biology, and † Division of Engineering and Applied Sciences, Harvard University, Cambridge, Massachusetts 02138, USA*

Carbon nanotubes[1] are predicted to be metallic or semiconducting depending on their diameter and the helicity of the arrangement of graphitic rings in their walls[2–5]. Scanning tunnelling microscopy (STM) offers the potential to probe this prediction, as it can resolve simultaneously both atomic structure and the electronic density of states. Previous STM studies of multi-walled nanotubes[6–9] and single-walled nanotubes (SWNTs)[10] have provided indications of differing structures and diameter-dependent electronic properties, but have not revealed any explicit relationship between structure and electronic properties. Here we report STM measurements of the atomic structure and electronic properties of SWNTs. We are able to resolve the hexagonal-ring structure of the walls, and show that the electronic properties do indeed depend on diameter and helicity. We find that the SWNT samples exhibit many different structures, with no one species dominating.

The diameter and helicity of a defect-free SWNT are uniquely characterized by the vector $\mathbf{c_h} = n\mathbf{a_1} + m\mathbf{a_2} \equiv (n, m)$ that connects crystallographically equivalent sites on a two-dimensional graphene sheet, where $\mathbf{a_1}$ and $\mathbf{a_2}$ are the graphene lattice vectors and n and m are integers (Fig. 1). Electronic band structure calculations[2–5] predict that the (n,m) indices determine the metallic or semiconducting behaviour of SWNTs. Zigzag $(n,0)$ SWNTs should have two distinct types of behaviour: the tubes will be metals when $n/3$ is an integer, and otherwise semiconductors[3–5]. As $\mathbf{c_h}$ rotates away from $(n,0)$, chiral (n,m) SWNTs are possible with electronic properties similar to the zigzag tubes; that is, when $(2n + m)/3$ is an integer the tubes are metallic, and otherwise semiconducting. The gaps of the semiconducting $(n,0)$ and (n,m) tubes should depend inversely on diameter. Finally, when $\mathbf{c_h}$ rotates 30° relative to $(n,0)$, $n = m$. The (n,n) or armchair tubes are expected to be truly metallic with band crossings at $\mathbf{k} = \pm 2/3$ of the one-dimensional Brillouin zone. It has been suggested that SWNT samples produced by laser vaporization[11] and arc[12] methods consist predominantly of (10,10) metallic armchair tubes.

We have carried out STM measurements in ultra-high vacuum at 77 K on purified SWNT samples produced by laser vaporization[11]. Typical atomically resolved images of a SWNT on the surface of a rope, which consists of parallel tubes[11], and isolated SWNTs on a Au(111) substrate are shown in Fig. 2a and b, respectively. Figure 2a shows the expected honeycombe lattice for a SWNT with a C–C spacing of 0.14 ± 0.02 nm. The chiral angle is readily determined by identifying the zigzag tube axis direction (the line connecting sites separated by 0.426 nm) relative to the sample tube axis. This shows quite clearly that the tube is chiral with an axis orientated at an angle of −8.0 ± 0.5° relative to that for a zigzag nanotube. As the tube axis is perpendicular to $\mathbf{c_h}$, this corresponds to the angle between $\mathbf{c_h}$ and $(n,0)$ in Fig. 1. From this angle and the measured diameter of 1.0 ± 0.05 nm, we can assign (n,m) indices of either (11,2) or (12,2); the angle/diameter for (11,2) and (12,2) are −8.2°/0.95 nm and −7.6°/1.03 nm, respectively. We note that an (11,2) tube is expected to be metallic, whereas a (12,2) tube should be semiconducting. The helicity of the lower isolated SWNT in Fig. 2b was determined in a similar manner, yielding a chiral angle of −11.0 ± 0.5°; the diameter of this tube is 1.08 ± 0.05 nm. These parameters match closely the values expected for a (12,3) tube, ±10.9°/1.08 nm, and reasonably exclude other choices of indices.

Central to the work reported here is our ability to characterize the electronic properties of the atomically resolved nanotubes by tunnelling spectroscopy. Specifically, current (I) versus voltage (V) was measured at specific sites along the tubes and differentiated to yield the normalized conductance, $(V/I)\mathrm{d}I/\mathrm{d}V$, which has been shown[13] to provide a good measure of the main features in the local density of electronic states (LDOS) for metals and semiconductors. The gradual increase in current in the I–V data (Fig. 2c, d) recorded on the SWNTs imaged in Fig. 2a, b shows qualitatively that both tubes are metallic. The LDOS determined from data sets recorded at different locations along the tubes are very similar, demonstrating the reproducibility of the measurements; furthermore, the LDOS for both tubes are roughly constant between −600 and +600 mV as expected for a metal. Small variations in the LDOS with energy are not significant and arise from noise in the data. These spectroscopy results are similar to those obtained on the Au(111) substrate except that the surface state 450 meV below the Fermi level[14] is also observed on the latter.

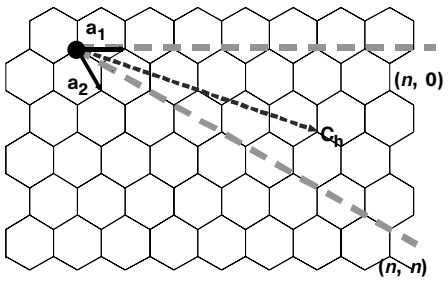

Figure 1 Schematic of a two-dimensional graphene sheet illustrating lattice vectors $\mathbf{a_1}$ and $\mathbf{a_2}$, and the roll-up vector $\mathbf{c_h} = n\mathbf{a_1} + m\mathbf{a_2}$. The limiting cases of $(n,0)$ zigzag and (n,n) armchair tubes are indicated with dashed lines. As represented here, the angle between the zigzag configuration and $\mathbf{c_h}$ is negative.